PCCP

PAPER

Interplay between the ionic and electronic transport and its effects on the reaction pattern during the electrochemical conversion in an FeF_2 nanoparticle

Cite this: *Phys. Chem. Chem. Phys.*, 2014, **16**, 11690

Ying Ma and Stephen H. Garofalini*

Received 31st January 2014,
Accepted 1st April 2014

DOI: 10.1039/c4cp00481g

www.rsc.org/pccp

Using a charge dependent embedded atom method potential in conjunction with a dynamically adaptive multibody force field, the conversion reaction in an iron difluoride nanoparticle exposed to lithium ions is investigated. The reactions take advantage of the multiple valence states of the cations. A subtle interplay between the ionic and electronic transport, which is not accessible in conventional fixed-charge simulations, has been revealed. The simulated reaction pattern is in close agreement with that observed experimentally at the nanoscale, while providing detailed atomistic mechanisms. Due to difference in the ionic and electronic transport, different stages of reaction are observed and the corresponding phase growth mechanisms have been identified. Initially local Li concentration plays a key role in driving the reaction through amorphous reaction products to the crystalline phases that inhibit Li transport. However, electronic transport and interfacial ion diffusion are shown to be important in creating further transport pathways that allow continued conversion reactions, providing the mechanism that enables the use of these materials in advanced high capacity lithium ion batteries. Such interplay between the ionic and electronic transport will also be important in other materials and devices for energy conversion and storage.

1. Introduction

Conversion compounds are among the most promising materials for next generation batteries with higher energy and power densities.[1–4] Such compounds have at least double, sometimes even triple, theoretical capacities.[5–9] When used as electrodes in a lithium ion battery (LIB), a conversion reaction occurs in these materials upon charging or discharging. The enhanced capacity rests in the ability to access the various valence states of the metal cation during the conversion. Furthermore, excellent capacity retention and reversibility have been demonstrated in a few model systems.

Iron difluoride (FeF_2) is among the most studied conversion compounds in which the following conversion reaction occurs:

$$2Li^+ + FeF_2 + 2e^- \rightarrow 2LiF + Fe \quad (1)$$

A number of experimental techniques including high resolution transmission microscopy (HRTEM),[10] electron energy loss spectroscopy (EELS),[11] X-ray pair distribution function (PDF) analysis,[12] have been employed to identify the local structure and phase evolution during the conversion reaction in FeF_2. A recent study reveals an inter-connected iron network in converted FeF_2 which is believed to provide the electronic conduction pathway required for reconversion.[10] With a newly developed *in situ* electrochemical cell, lithium transport has been tracked in individual FeF_2 particles at the nanoscale.[13] Computational studies have also been performed at different time and length scales. Assuming a spinodal type growth mechanism, a recent phase field simulation gives a micro-structure of converted FeF_2 in close resemblance of that observed experimentally.[13] The initial formation of a glassy LiF network followed by nanocrystal formation was first predicted by a molecular dynamics (MD) simulation[14] using a reactive force field and then confirmed experimentally.[13] First principles calculations based on the density function theory (DFT) have also been used to identify possible reaction paths, although the actual path may deviate from the predicted equilibrium path.[15,16] These combined experimental and computational efforts have greatly enhanced our knowledge of the conversion reaction but key issues such as the ionic and electronic transport mechanisms and pathways remain undetermined. For example, MD simulations that reproduce the formation of the crystalline Fe-metal nanoclusters and LiF crystal during conversion also show the self-limiting nature of the conversion.[14] Additional reaction pathways must exist for continued conversion. Furthermore, the actual roles of ionic and electronic transport are still mysterious, and the mechanisms leading to the unique morphology observed experimentally[13] are not fully understood.

Department of Materials Science and Engineering, Rutgers University, 607 Taylor Rd, Piscataway, NJ 08854, USA. E-mail: shg@rutgers.edu

Answers to these questions are critical to our understanding of the conversion reaction, unfortunately are undeterminable experimentally, hence requiring MD simulations using an accurate reactive force field.

In this work, a charge dependent embedded atom method (Q-EAM) is developed in concert with a dynamically adaptive reactive force field.[14] With this approach, the conversion reaction in an FeF_2 nanoparticle is studied. The interfaces between FeF_2 and the electrolyte are ignored since the current study concerns Li starting at the nanoparticle surface, the reaction within the FeF_2 nanoparticle, and transport in the product phases. A clear atomistic picture of the reaction is revealed, and the nanostructures that evolve in the simulations are in close agreement with those observed experimentally.[13] More importantly, while electronic conduction is generally not accessible by an MD simulation, we show here that by utilizing this dynamically adaptive approach, the role of both ionic and electronic transport during the conversion can be identified. The ionic transport is observed to depend subtly on the electronic transport. Different transport pathways are observed at different stages of conversion, which is closely related to the local structures formed during the reaction. The effects of interfacial diffusion have also been explored and are believed to be important in determining the final geometry of the converted structure.

2. Theory and model

2.1 The charge dependent embedded atom model (Q-EAM)

Metallic iron forms during the conversion reaction in iron fluoride. The embedded atom method (EAM) has been widely used in the simulation of metals including iron. EAM potentials have the general form as given below:

$$E^{\mathrm{EAM}} = \frac{1}{2}\sum V_{\mathrm{ij}} + \sum F(\rho_{\mathrm{i}}) \quad (2)$$

where V_{ij} is the pair energy function between atom i and j, and F is the embedding energy which is a function of the electron density ρ_i. The electron density is defined as:

$$\rho_{\mathrm{i}} = \sum \rho_{\mathrm{ij}}(r_{\mathrm{ij}}) \quad (3)$$

where ρ_{ij} is the contribution to the electron density of atom i from atom j separated by a distance r_{ij}.

In this work, the EAM potential reported by Chamati *et al.*[17] was used. However, the Fe bonding may be significantly different from a metallic one during the conversion reaction. For example, Fe atoms close to Fe/FeF_2 interfaces may be positively charged due to possible charge transfer between Fe atoms and their neighbouring F atoms. In this case, the Fe bonding becomes partially ionic, which is beyond the capability of general EAM potentials. To this end, a charge dependent embedded atom model is developed by introducing a charge dependent switching function f_{ij}, as given below:

$$E^{\text{Q-EAM}} = \frac{1}{2}\sum f_{\mathrm{ij}} V_{\mathrm{ij}} + \sum F(\rho_{\mathrm{i}}) \quad (4)$$

$$\rho_{\mathrm{i}} = \sum f_{\mathrm{ij}} \rho_{\mathrm{ij}} \quad (5)$$

$$f_{\mathrm{ij}} = \frac{1}{2}\mathrm{erfc}\left(\left(\frac{q_{\mathrm{i}} + q_{\mathrm{j}}}{2} - 0.55\right)\Big/0.22\right). \quad (6)$$

When charges are all zero, the switching function approaches one and it reduces to the original EAM potential.

Furthermore, as metallic iron forms during conversion, a potential is required which is able to evolve continuously from the ionic bonding in FeF_2, which is described by the sum of a short range repulsion E^{rep} and electrostatic interaction E^{ele},[18] to the metallic one in iron as described by the Q-EAM potential. Thus, the Fe–Fe potential is written as follows:

$$E_{\text{Fe–Fe}} = (1 - f_{\mathrm{ij}})E^{\mathrm{rep}} + E^{\text{Q-EAM}} + E^{\mathrm{ele}} \quad (7)$$

Although a similar approach has been previously reported,[14] the metal potential employed failed to reproduce the correct body-centered cubic (BCC) structure of the metallic iron formed during the conversion. The current approach, on the other hand, reproduces accurately the crystalline structures of all the phases involved in the reaction. Furthermore, the previous potential predicted surface energies that are two times larger than the experimental data. Since the reaction is initiated on the surface, a proper description of surface energetics is important to correctly reproduce the reaction pattern. This new potential leads to greatly improved surface energies. The details of the surface energy calculations have been previously reported,[18] and the calculated surface energies are summarized in Table 1, along with available experimental and theoretical data.[19,20]

To further test the validity of the current potential, first principles DFT calculations are performed to obtain the ionic diffusion barriers since no experimental data are available. However, due to computational restrictions, only the lithium diffusion barrier in perfect lithium fluoride (LiF) crystal is calculated and compared with the MD result, while the rest of the data are predicted by MD simulations. The DFT calculations are performed using the nudged-elastic band method as implemented in the Vienna ab initio Simulation Package (VASP).[21,22] The projector augmented wave method[23] is used and the exchange correlation potential is described by a generalized gradient approximation with the Perdew–Burke–Ernzerhof parameterization.[24]

2.2 Simulation methods

The diffusion barriers of Li in FeF_2 were previously reported.[14] Since those previous simulations showed a slowdown of the conversion process after formation of the crystalline LiF and Fe-metal products, the diffusion of Li in these product phases is

Table 1 Calculated surface energies (J m^{-2})

		MD	DFT	Exp.	Theory
FeF_2	(001)	0.76	0.50	—	
	(110)	0.60	0.36	—	
Fe	(001)	2.46	2.38	2.36[19]	
	(110)	2.23	—		
	(111)	2.64	—		
LiF	(001)	0.72	0.32		0.20–0.5[20]

performed here, along with conversion in FeF_2 nanoparticles. The role of F diffusion is not considered in this work since it is less important compared to Li diffusion and F migration distances are minor. It is the Li that must enter the crystal to reach the F. At early stages of reaction, the reaction is driven by Li diffusion. After the formation of crystalline LiF, continued reaction requires transport of Li instead of F to regions inside the particle.

To study the diffusion barrier in bulk LiF, a lithium ion is placed in a channel. Due to the cubic symmetry of LiF, diffusion along the [100], [010] and [001] channels are all equivalent. For simplicity, only diffusion along [001] channel is reported. The crystallographic directions [100], [010] and [001] are denoted as x, y, and z, respectively. The lithium ion is then moved incrementally along z by 0.02 Å. At each z coordinate, a damped molecular dynamics approach is used to minimize the total energy of the system. The x and y coordinates of the diffusing ion are allowed to relax while z is kept fixed. The charge of the diffusing Li ion is determined according to the electronegativity equalization principle.[25,26] It should be pointed out that the electronegativity equalization method assumes no electronic barrier[27] such that the charge on the Li^+ ion is able to reach its equilibrium value. However, both the reactant (FeF_2) and the product (LiF) are electronically insulating and significant electronic transport is not expected (except after the formation of metallic iron). Considering, for example, a relatively simple case where a Li^+ diffuses in a bulk LiF crystal, the interstitial Li^+ creates a defect level close to the conduction band minimum (CBM). Since LiF has a large band gap of 13.6 eV,[28] it is unlikely that any electrons in the valence band can be excited to the defect level. In other words, a Li ion will remain as an ion unless an electron diffuses from outside to the vicinity of this ion. For this reason, a fixed Li charge model is also studied where the charge of the diffusing Li^+ is kept constant at 0.84, which is the equilibrium charge of a Li ion in LiF. However, the rest of the system is relaxed according to the electronegativity equalization principle since no electronic transport is required during the charge equilibration. Comparison of the two scenarios could give an indication of the effects of electronic transport during the reaction, which is otherwise not accessible in traditional fixed charge simulations where all the atomic charges are fixed during the simulation (*i.e.* no charge transfer or transport).

In some cases an exchange between this original diffusing Li and a lattice Li occurs in which two scenarios are used: one in which this initial Li is continually moved, and two, after the exchange, the exchanged Li that is now in a channel is moved and not the original Li. Exchange is only observed in the case of using a fixed-charge Li ion, so after exchange, whether the original Li is continued to be moved or the exchanged Li is moved, either is moved as a fixed-charge Li. In the case of surface diffusion, the Li ion is placed 2 Å above the surface and then marched into the surface. In all cases, the energy of the system as a function of the diffusion length is recorded and the diffusion barrier is calculated at the end of each relaxation step.

MD simulations are then used to study the conversion reaction in an FeF_2 nanoparticle. The actual shape of a nanoparticle depends on the surface energies, preparation history, *etc.* For simplicity, we choose two low energy surfaces (001) and (110) to construct the particle which is terminated with (001) surface along $\pm z$ direction and (110) surfaces along $\pm x$ and $\pm y$ directions. For comparison, a larger particle with a size of 5 nm × 5 nm × 5 nm and a smaller particle of 3 nm × 3 nm × 3 nm are studied. The particles are first relaxed in vacuum for 30 ps, then reflecting boundaries are added around 1.5 Å away from each surface of the particle. During discharge in real systems, there is an energy lowering which drives Li ions from the anode to the cathode, and Li^+ ions are inserted into the FeF_2 particles from the carbon matrix. Since the current simulation only considers the cathode, such a process is simulated by randomly generating Li^+ ions along the reflecting boundaries. For real systems, transport is also limited by the behaviour of electrolytes and electrolyte/electrode interfaces. Experimentally, the electrode reaction is very fast, but at a macroscopic scale. It is not possible to simulate such a timescale from MD. As a result, our MD simulations are based on a very high reaction rate by adding lithium directly to the system. The reflecting boundary is used to prevent any added Li ions from leaving the interface region, enabling them to react with the nanoparticle. For the smaller particle, a complete discharge requires 3456 Li^+ ions that are generated at a rate of 36 Li^+/10 ps. For the larger particles, 8192 Li^+ ions are required for a complete discharge, and a rate of 64 Li^+/10 ps is studied. The positions of the reflecting boundaries are changed to allow for volume expansion during the reaction. In our simulations, volume expansion of around 40% is observed. The evolution of the structure is then recorded and analyzed. For all the MD simulations, a time step of 1 fs is used.

3. Results and discussion

3.1 Li diffusion barrier in bulk LiF

Since the whole reaction depends critically on Li transport, the Li diffusion barrier in a LiF crystal was first calculated. The general observation is that LiF is not a good ionic conductor, which has been previously confirmed by both MD simulations[14] and experimental observations.[29] As previously shown,[14] the conversion reaction that very quickly initiates on the FeF_2 surface upon exposure to Li ions is significantly slowed down after the formation of crystalline LiF and Fe, consistent with a high diffusion barrier. Surprisingly, DFT calculations give a relatively small diffusion barrier of Li in bulk LiF, as shown in Fig. 1.

In MD simulations, electronic transport seems to have profound impact on the barrier. Assuming no barrier for electronic transport such that an electron diffuses into the system and reaches equilibrium, a small barrier of 0.30 eV is observed, close to the DFT barrier of around 0.45 eV. The charge on the diffusing Li^+ is partially reduced to around 0.6 with this compensating electron. However, it is also possible that electronic transport is slow and the charge on the diffusing Li ion cannot be equilibrated, creating the fixed Li charge model. Note that it is different from a conventional fixed-charge simulation since the rest of the system is charge relaxed. In this case, after an initial small barrier, a sudden decrease is observed, followed by a large increase of the barrier to around 1.2 eV. The sudden

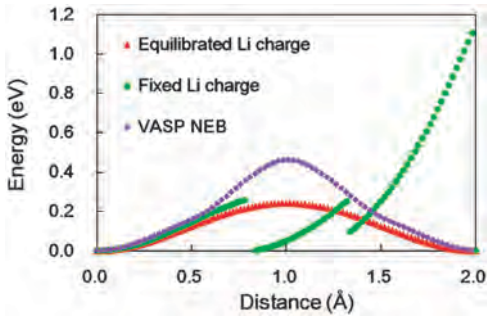

Fig. 1 Li diffusion bulk in bulk LiF. Only the initial Li is moved here.

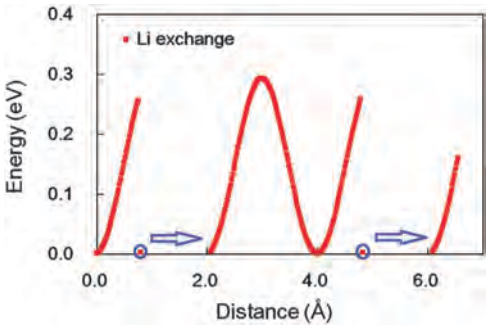

Fig. 3 Li^+ bulk diffusion barrier with exchange mechanism. Circles indicate the position of an exchange. Arrows show that during the exchange, the new diffusing Li^+ has moved forward along the diffusion direction and after exchange its energy is monitored, thus leading to a sudden increase in the *x*-axis distance coordinates.

decrease in energy involves an exchange of the diffusing fixed-charge Li^+ with a Li on a nearby lattice site. The atomistic configurations during an exchange are shown in Fig. 2. Initially, the Li ions close to the diffusing Li deviate slightly from their equilibrium positions (Fig. 2(a)). As the diffusing Li continues to move along *z*, those Li ions are pushed farther away (Fig. 2(b)) until the exchange takes place where a Li ion at a lattice site is knock out to a nearby channel and the site is occupied by the original diffusing Li ion (Fig. 2(c)). This originally diffusing Li^+ is trapped in the lattice site and further diffusion of this ion is limited by the large 1.2 eV barrier. Of course, the ion that is knocked out from its original lattice site is now ready to diffuse and its charge is now fixed. The barrier is quite small (0.3 eV), although it cannot diffuse far before another exchange takes place (Fig. 3). Note the difference between the *x*-axis in Fig. 1 and 2. The unit cell dimension is 4 Å in this direction and the exchange occurs only in the first 2 Å of each cell. These observations suggest a subtle interaction between ionic and electronic transport, which may in turn affect phase separation and the reaction pattern. Even in the case of the fixed Li charge model, considerable Li diffusion in LiF is expected through the exchange mechanism, although the speed would be lower than a direct diffusion mechanism.

3.2 Li diffusion barrier into LiF surface

For Li to enter the LiF crystal, it must diffuse from outside the surface. While a real system would have electrolyte or carbon matrix adjoining the cathode, the Li^+ ion must still enter the LiF crystal from a surface if transport through crystalline LiF occurs and the current simulations only evaluate this scenario. Calculations of diffusion of Li into the crystal from the outer surface show that there is a large barrier that prevents Li^+ from entering into the crystal, as shown in Fig. 4. Similar behavior showing that a large surface barrier is accompanied by a small bulk barrier has recently been reported for Li insertion in manganese oxides.[30] In the case where the charge on Li is equilibrated, a barrier of around 1.0 eV is observed before the exchange of the diffusing ion and the lattice ion. After exchange, further diffusion of the original Li^+ ion is again faced with a large barrier. In the case of fixed Li charge, a smaller barrier of 0.6 eV is observed before exchange, followed by a large 2.5 eV barrier. Interestingly, the exchange mechanism on the surface is quite different from that in the bulk. In the latter case, the lattice atom is knocked out and pushed farther along the diffusion direction, thus enabling continued low-barrier diffusion. In the case of surface diffusion, the lattice atom is not knocked into the crystal after exchange but rather is knocked up to a terrace adsorption site, as shown in Fig. 5(b), with the energy barrier shown in Fig. 5(a). Further diffusion of the knocked out atom into the crystal will then occur with the same barrier as the original diffusing Li until another lattice atom is knocked away, again, from the surface. In other words, Li does not readily diffuse into the bulk, which explains the lack of Li conductivity observed experimentally. For the same reason, Li transport through iron (Fe) crystals is also not possible. Indeed, an even higher surface barrier is observed in the simulated diffusion of Li into the Fe crystal.

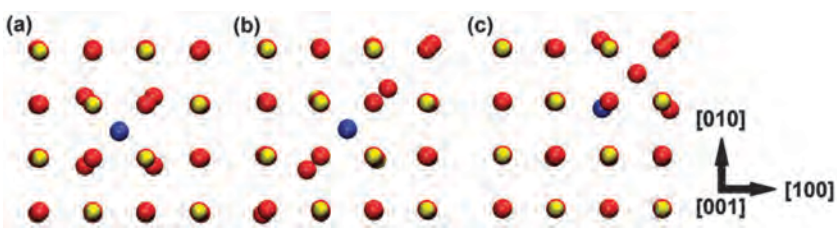

Fig. 2 Atomic configurations during an exchange viewed along [001] direction. Red and yellow spheres are Li and F ions at lattice sites, while blue sphere is the diffusion Li^+ in the diffusion channel. (a) Initial configuration. Li ions close to the diffusion ion is slightly pushed away from their equilibrium sites. (b) Configuration before exchange and (c) configuration after exchange where the diffusion ion is attracted into a lattice site kicking a Li ion into the channel. (a) and (c) are energetically equivalent, while (b) is at a higher energy which gives the barrier for exchange.

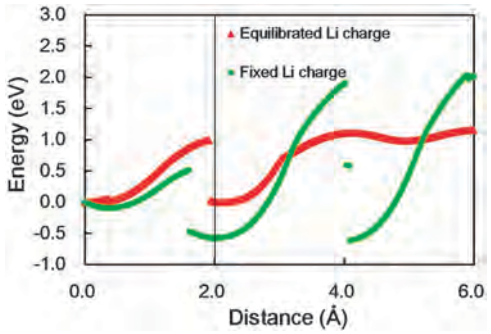

Fig. 4 Li^+ diffusion barrier on a LiF surface. Vertical solid line denotes the location of LiF surface at 2 Å, bulk LiF is at larger distances. Li adatom started at 0 Å. In both cases, a surface barrier builds up which prevents Li^+ from entering into the bulk. In the case of fixed Li charge, the surface barrier is smaller (0.6 eV), however followed by a 2.5 eV barrier below the surface. Large drops in energy caused by diffusing Li exchanging with lattice Li.

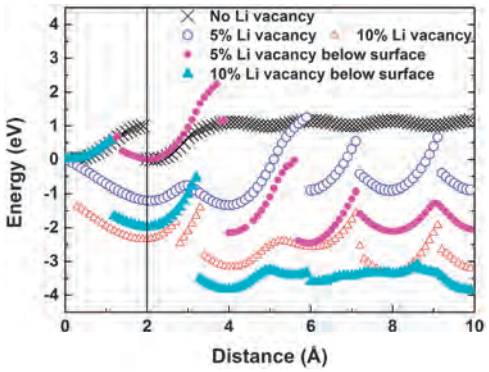

Fig. 6 The effects of Li-deficiency on the Li surface diffusion barriers. Vertical solid line denotes the location of LiF surface at 2 Å, bulk LiF is at larger distances. Li adatom started at 0 Å.

It should be noted that crystalline LiF and Fe^0 clusters form only at the later stage of the conversion. Our previous studies show that Li can diffuse from the (001) surface down the open channels in FeF_2 with a small barrier, with simultaneous structural instabilities at the surface that enable Fe^0 clusters to form.[14] Clustering of Fe leaves under-bonded F ions that form a Li–F network region with the incoming Li ions. The Li–F network is highly Li-deficient and is amorphous, enabling additional Li ions to transport through this structure into the subsurface.[14] Our prediction of the presence of this amorphous phase was corroborated in subsequent experiments.[13] It is thus important to identify the effect of Li deficiency in LiF on the diffusion barrier. To this end, different concentrations of Li vacancies are generated by randomly removing Li lattice sites in a LiF crystal. The Li-deficient structure is then relaxed and the Li surface diffusion barrier is studied. It is expected that the diffusion process is more complicated due to the existence of Li vacancies. The diffusing atom can not only exchange with a lattice atom, but also be attracted to a vacancy site. This complexity leads to large fluctuations in the energies as shown in Fig. 6.

3.3 The conversion reaction in an FeF_2 nanoparticle

The most important feature is that the surface barrier disappears and a driving force builds up which enables Li diffusion. Increased vacancy concentration leads to increased driving forces. This feature clearly suggests the importance of Li concentration in determining the ionic transport during the reaction. For a numerical description of the local Li concentration, we define the Li/F ratio as the ratio of the number of Li to that of F within the third neighbour distance of each species. Such a ratio is close to 1 in a perfect LiF crystal. The reaction in a 3 nm × 3 nm × 3 nm FeF_2 nanoparticle exposed on all six sides to Li ions is simulated and the evolution of the local Li/F ratio is shown in Fig. 7. For a detailed view of the reaction, snapshots at the corresponding stages of the reaction are shown in Fig. 8. Initially, Li^+ ions diffuse within the FeF_2 channels and no Li–F bond forms (the starting FeF_2 configuration is given in Fig. 8(a)). At this stage, the barrier to Li^+ diffusion in FeF_2 is small, and no significant change in the parent FeF_2 structure is observed which seems to support the existence of an intercalation stage. The experimental evidence for this initial intercalation stage is scarce and it is argued that direct Li intercalation into FeF_2 is not possible since reduction of Fe^{2+} to Fe^{1+} is unlikely. A recent solid state

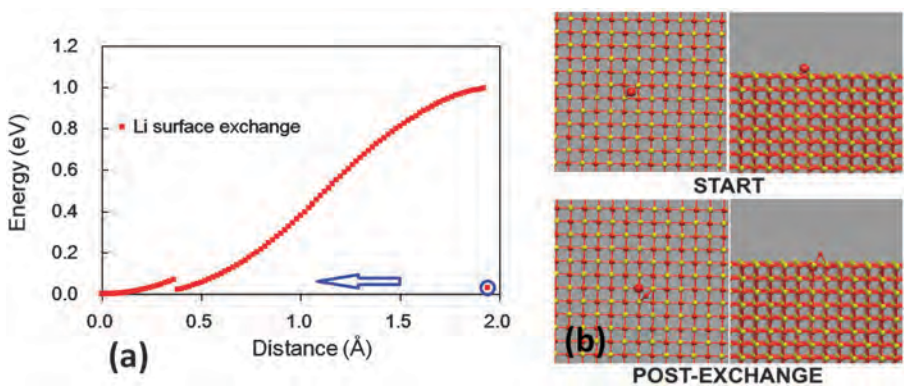

Fig. 5 (a) Energy of Li^+ surface exchange. Circles indicate the position of the exchange. Arrows show that after exchange, the new diffusion atom is pushed away from the surface. Surface locates at 2.0 Å. (b) Top (left) and side (right) views of the inserting Li (large red) exchanging for the lattice Li (small red) in LiF crystal surface. Yellow are F ions.

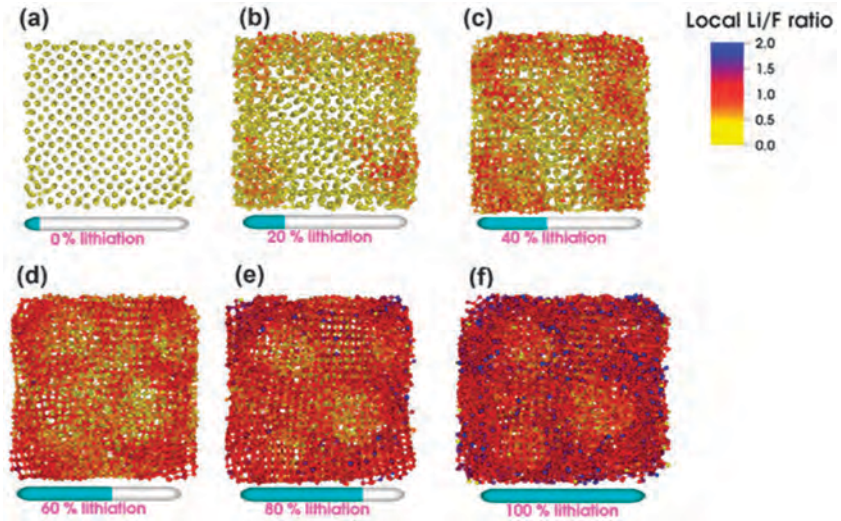

Fig. 7 Evolution of the local Li concentration during a conversion reaction in an FeF_2 nanoparticle. A ratio of 1.0 indicates the correct stoichiometry in a LiF crystal. Smaller ratio indicates Li deficiency and larger ratio indicates Li segregation. Empty regions are occupied by Fe clusters (not shown).

NMR study indicates the existence of an initial intercalation, although it is justified by an *assumed* presence of Fe^{3+} impurities.[12] However, as we have shown previously,[14] insertion of a Li^+ does not necessary mean reduction of a *single* Fe^{2+} to Fe^{1+}. Both DFT and MD simulations show that when a Li^+ ion diffuses into FeF_2, the accompanying electron is shared among multiple nearby Fe^{2+} ions as observed by a slight decrease in their atomic charges.[14] In other words, Li intercalation is supported by changes in the local electronic structure. However, such changes lead to structural instabilities in the Fe–F bonding. As more Li^+ ions arrive, charges on some Fe^{2+} ions are further decreased which effectively is equivalent to a 1+ state. Such a state is unstable and is immediately reduced to zero as seen by the breaking of Fe–F bonds. These reduced Fe^0 atoms are attracted toward each other and form the nuclei upon which Fe nanoparticles grow. At the same time, Li–F bonds are observed. Distribution of the bonded Li–F region is roughly uniform on the surface as Li^+ enters the FeF_2 parent particle randomly. The structure of the Li–F region is amorphous since Li^+ is deficient and the local Li/F ratio is only around 0.5 (Fig. 7(b)). Fe^0 clusters also show an amorphous structure (Fig. 8(b)). Driven by surface energy reduction, some initial coarsening of the smallest Fe^0 clusters is observed. At this early reaction stage, all of the clusters are relatively small with a diameter less than 1 nm,

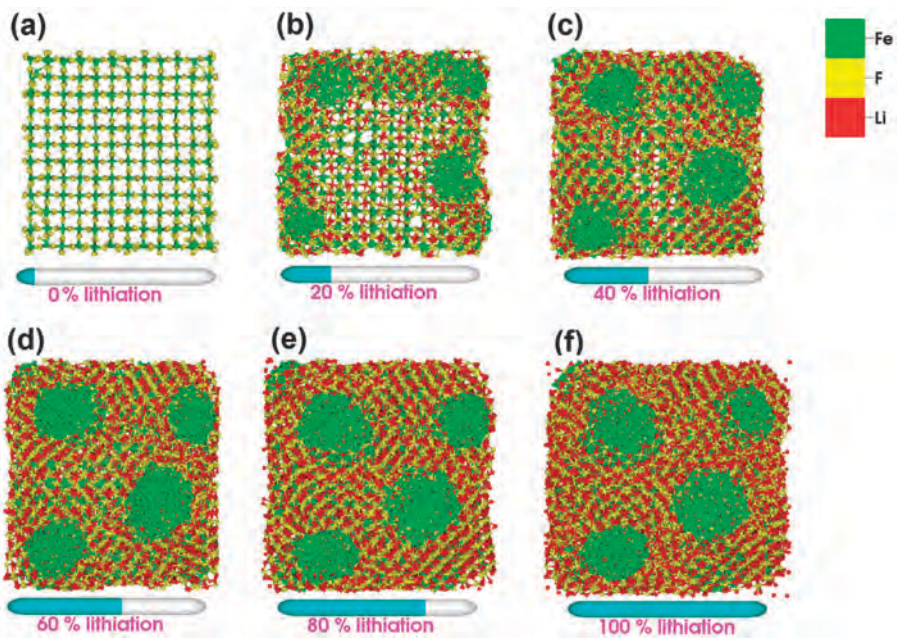

Fig. 8 Structural evolution of an FeF_2 nanoparticle exposed on all sides to Li ions during a conversion reaction (red = Li, yellow = F, green = Fe). Notice that only one surface is depicted, the pattern is similar on other surfaces.

consistent with experimental observation.[13] As indicated from the above calculations on the surface driving forces in defective LiF, substantial Li^+ transport is expected through the Li-deficient region that results in a steady increase in the local Li/F ratio. Once this ratio is close to 1.0, crystalline LiF regions are observed (Fig. 7(c and d)). Some crystalline region has also been observed in Fe^0 clusters (Fig. 8(c)).

It seems that the reaction would have stopped here due to the surface barrier after the formation of crystalline LiF, leaving FeF_2 underneath the surface region unreacted. Notice that the Fe clusters are rather small (Fig. 8(c) where the size of the system is ~3 nm) and are randomly distributed on the surface region at this stage. Coarsening of the Fe nanoparticles is also not possible since Fe atoms cannot diffuse through the crystalline LiF region. It can be seen from Fig. 8 that after formation of the LiF crystal, only limited lateral growth of the Fe clusters is observed (Fig. 8(c–f)). Indeed, continued addition of Li ions causes Li^+ segregation on the outer surface, as seen by the increase of the local ratio from ~1.5–2.0 (Fig. 7(d–f)). However, although much slower, the reaction does not stop as evident from the further growth of the polycrystalline LiF region (Fig. 7(d–f) and 8(d–f)), which suggests the existence of other diffusion channels. The only such channels left are thus the interfaces between the crystalline LiF and the Fe cluster. To identify the possible interfaces, interfacial energies for different combinations of LiF and Fe orientations are studied and the results are listed in Table 2. The Li^+ diffusion barriers along these interfaces are also studied. All the barriers are quite high (around 2.0 eV) except for one case: Li^+ diffusion along the Fe(111)/LiF(001) interface, as shown in Fig. 9. Again, electronic transport seems to play an important role here. If the charge on the diffusing Li^+ is fixed, a large barrier of 1.0 eV is observed. On the other hand, the barrier reduces to 0.3 eV if the charge on the Li^+ is equilibrated by migration of a compensating electron. Would it be possible for the electrons to reach the interfacial region and thus reduce the Li^+ diffusion barrier? If possible, what's the electronic transport path? The newly formed Fe crystalline region could provide sufficient electronic conductivity to allow electrons to reach the interfacial region. As more Li ions arrive at the reaction front through the interface, FeF_2 below the surface reaction region starts to decompose. Reduced Fe atoms are attracted toward the Fe cluster, while Li and F are attracted toward the LiF crystal for further growth. As such, the reaction front propagates into the bulk, and both Fe and LiF crystals continue to grow. In other words, the Fe nanoclusters are able to grow inward rather than coarsen laterally with their neighboring clusters because that is prohibited by the LiF phase separating them. As the inward growth continues, some Fe clusters from different surfaces come into contact and form a percolated structure. Also the orientation of the Fe clusters is largely coherent, which could be a result of the limited diffusion of Fe. Since a single grain of the FeF_2 is studied, as the Fe^{+2}-sublattice in the parent FeF_2 structure collapses, the BCC structures that form share the same orientation.[13] Such a process requires the minimal Fe diffusion. Upon full conversion, a continuous, coherent Fe network forms as shown in Fig. 10. Notice that the sizes of the Fe particles are generally around 1–3 nm, which is also consistent with experimental observation.[13] The interconnected Fe network is believed to be important in the reversibility of the reaction. Such a unique morphology is thus largely a result of the interplay of ionic and electronic transport along the Fe/LiF interfaces.

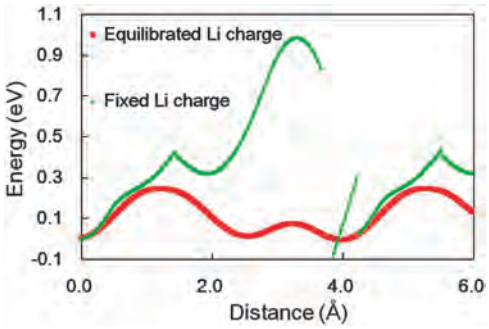

Fig. 9 Li^+ diffusion barrier along the Fe(111)/LiF(001) interface.

Furthermore, this subtle interplay between the ionic and electronic transport seen in these simulations also determines the structures of the Fe/LiF interfaces. The final interfacial geometry is dominated by both the Fe(110)/LiF(001), which is expected due to its smaller interfacial energy, and the Fe(111)/LiF(001) interfaces. The fact that such a high energy interface exists is quite interesting and we believe it is largely an effect of the electronic transport. Initially, when the Fe/LiF interface forms, it is expect that most of them are Fe(110)/LiF(001) interfaces since they are energetically more favorable. However, the interfacial diffusion barrier is extremely high for Li. The further growth of the Fe(110)/LiF(001) interface is thus limited. On the other hand, even though Fe(111)/LiF(001) is scattered initially, it provides an additional transport path and thus is able to grow even though the interfacial energy is relatively high. These observations demonstrate that the structures of the phases involved in such complex electrochemical reactions may differ significantly from their thermodynamic equilibrium.

Table 2 Calculated interface energies (J m^{-2})

Interfaces	Orientation	MD
Fe/LiF	(001)/(001)	2.59
	(111)/(001)	2.72
	(110)/(001)	2.04

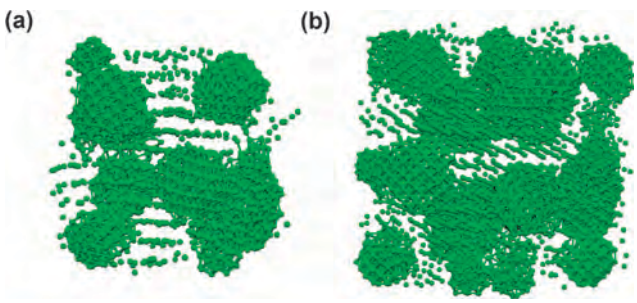

Fig. 10 The interconnected Fe network after reaction of FeF_2 to Li (LiF and remaining FeF_2 not shown here) for (a) a 3 nm × 3 nm × 3 nm cluster and (b) a 5 nm × 5 nm × 5 nm cluster.

The whole reaction can be divided into a "fast" initial intercalation stage, an intermediate surface reaction stage and a "slow" bulk reaction stage. Different transport pathways exist at different stages of reaction. The intercalation stage is supported by a change of the local electronic structure near the inserted Li^+, rather than the reduction of Fe^{2+} ions. At this stage, fast ionic transport is expected due to the existence of the low barrier open channels in the parent FeF_2 structure.[14] In the surface reaction stage, the Li concentration plays a key role and a driving force exists which enables continued ionic transport. However, this driving force decreases with increasing local lithium concentration that implies decreasing reaction speed. Electronic transport seems to be less important at this stage because it may be a surface phenomenon. In any case, significant electronic conduction is not possible since both the parent FeF_2 and the reactant LiF are insulating, although electronic transport is possible through, for example, defect or tunneling effect. However, with the growth of crystalline Fe^0 clusters and the formation of the continuous Fe^0 network, electronic transport is then effective in reducing the interfacial diffusion barrier that is important for the, albeit slow, bulk reaction and nearly complete conversion reaction observed experimentally.

4. Conclusion

The conversion reaction in FeF_2 nanoparticles has been studied by molecular dynamics simulation with a dynamically adaptive force field and the barriers to Li^+ transport relevant to the different stages of reaction have been determined. A complete atomistic picture of the conversion reaction that is consistent with available experimental observations is obtained. Different stages of reactions are identified, and the mechanisms are discussed. Furthermore, the role of ionic and electronic transport has been investigated, and a subtle interplay is found to determine the overall reaction pattern, which suggests the importance of considering both ionic and electronic transport when dealing with these kinds of complex electrochemical reactions.

Acknowledgements

This work was supported as a part of the Northeastern Center for Chemical Energy Storage, an Energy Frontier Research Center, funded by the US Department of Energy, Office of Basic Energy Sciences under award contract DE-SC0001294.

References

1 R. J. Brodd, in *Lithium-Ion Batteries: Science and Technology*, ed. M. Yoshio, R. J. Brodd and A. Kozawa, Springer, New York, 2009, p. 1.
2 J. M. Tarascon and M. Armand, *Nature*, 2001, **414**, 359–367.
3 J. Cabana, L. Monconduit, D. Larcher and M. R. Palacin, *Adv. Mater.*, 2010, **22**, E170–E192.
4 G. G. Amatucci and N. Pereira, *J. Fluorine Chem.*, 2007, **128**, 243–262.
5 H. Arai, S. Okada, Y. Sakurai and J. Yamaki, *J. Power Sources*, 1997, **68**, 716–719.
6 J. M. Tarascon, P. Poizot, S. Laruelle, S. Grugeon and L. Dupont, *Nature*, 2000, **407**, 496–499.
7 F. Badway, F. Cosandey, N. Pereira and G. G. Amatucci, *J. Electrochem. Soc.*, 2003, **150**, A1318–A1327.
8 H. Li, P. Balaya and J. Maier, *J. Electrochem. Soc.*, 2004, **151**, A1878–A1885.
9 H. Li, G. Richter and J. Maier, *Adv. Mater.*, 2003, **15**, 736–739.
10 F. Wang, R. Robert, N. A. Chernova, N. Pereira, F. Omenya, F. Badway, X. Hua, M. Ruotolo, R. Zhang, L. Wu, V. Volkov, D. Su, B. Key, M. S. Whittingham, C. P. Grey, G. G. Amatucci, Y. Zhu and J. Graetz, *J. Am. Chem. Soc.*, 2011, **133**, 18828–18836.
11 F. Cosandey, J. F. Al-Sharab, F. Badway, G. G. Amatucci and P. Stadelmann, *Microsc. Microanal.*, 2007, **13**, 87–95.
12 N. Yamakawa, M. Jiang, B. Key and C. P. Grey, *J. Am. Chem. Soc.*, 2009, **131**, 10525–10536.
13 F. Wang, H. C. Yu, M. H. Chen, L. Wu, N. Pereira, K. Thornton, A. Van der Ven, Y. Zhu, G. G. Amatucci and J. Graetz, *Nat. Commun.*, 2012, **3**, 1201.
14 Y. Ma and S. H. Garofalini, *J. Am. Chem. Soc.*, 2012, **134**, 8205–8211.
15 R. E. Doe, K. A. Persson, Y. S. Meng and G. Ceder, *Chem. Mater.*, 2008, **20**, 5274–5283.
16 G. Ceder, M. Aydinol and A. F. Kohan, *Comput. Mater. Sci.*, 1997, **8**, 161–169.
17 H. Chamati, N. I. Papanicolaou, Y. Mishin and D. A. Papaconstantopoulos, *Surf. Sci.*, 2006, **600**, 1793–1803.
18 Y. Ma, G. K. Lockwood and S. H. Garofalini, *J. Phys. Chem. C*, 2011, **115**, 24198–24205.
19 W. R. Tyson and W. A. Miller, *Surf. Sci.*, 1977, **62**, 267–276.
20 P. W. Tasker, *Philos. Mag. A*, 1979, **39**, 119–136.
21 G. Kresse and J. Furthmuller, *Comput. Mater. Sci.*, 1996, **6**, 15–50.
22 G. Kresse and J. Furthmuller, *Phys. Rev. B: Condens. Matter Mater. Phys.*, 1996, **54**, 11169–11186.
23 P. E. Blochl, *Phys. Rev. B: Condens. Matter Mater. Phys.*, 1994, **50**, 17953–17979.
24 J. P. Perdew, K. Burke and M. Ernzerhof, *Phys. Rev. Lett.*, 1996, **77**, 3865.
25 W. J. Mortier, S. K. Ghosh and S. Shankar, *J. Am. Chem. Soc.*, 1986, **108**, 4315–4320.
26 A. K. Rappe and W. A. Goddard, *J. Phys. Chem.*, 1991, **95**, 3358–3363.
27 R. A. Nistor and M. H. Muser, *Phys. Rev. B: Condens. Matter Mater. Phys.*, 2009, **79**, 104303.
28 D. M. Roessler and W. C. Walker, *J. Phys. Chem. Solids*, 1967, **28**, 1507–1515.
29 T. G. Stoebe and R. A. Huggins, *J. Mater. Sci.*, 1966, **1**, 117–126.
30 D. A. Tompsett, S. C. Parker, P. G. Bruce and M. S. Islam, *Chem. Mater.*, 2013, **25**, 536–541.